Electronic Supplementary Material (ESI) for RSC Advances.

pH-responsive superwetting nanostructured copper mesh film for separating both water-in-oil and oil-in-water emulsions

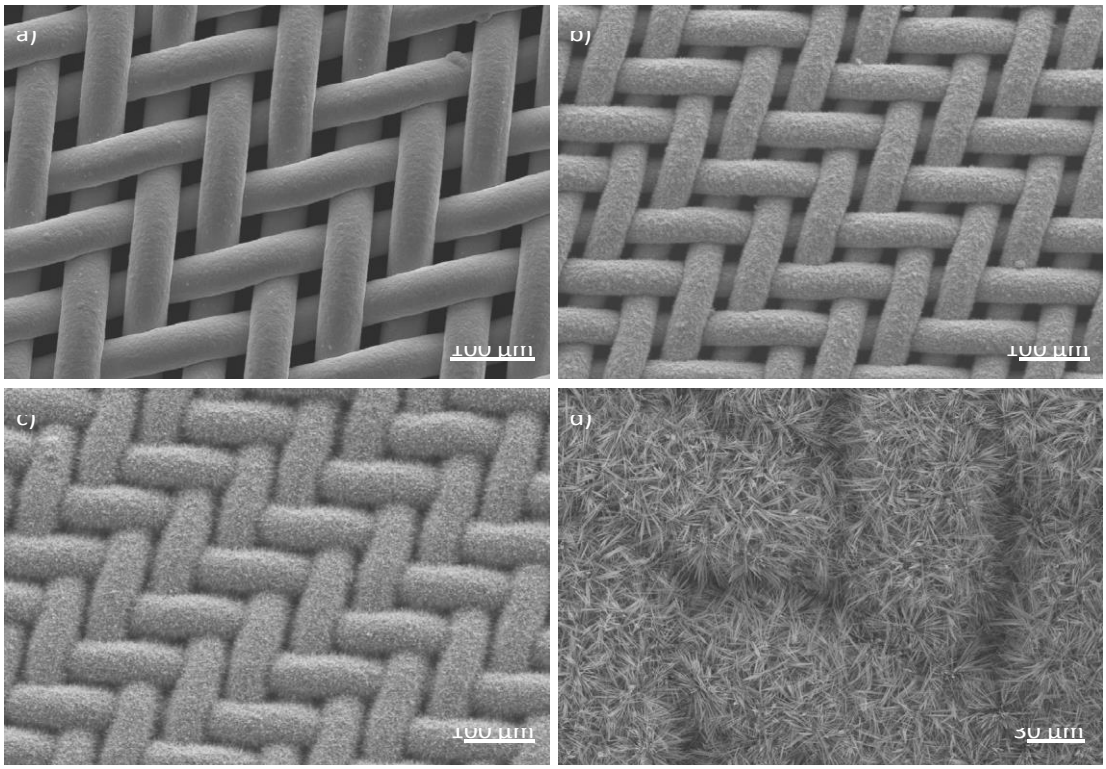

Figure S1. SEM images of copper mesh substrate after immersion into reaction solution for different times: (a) 0 min, (b) 10 min, (c) 20 min, and (d) 30 min, respectively. It can be seen that with increasing the reaction time, more $Cu(OH)_2$ nanowires can be produced on the substrate and when the time is about 30 min, no apparent pore can be observed on the substrate. Thus, in this work, reaction time 30 min was chosen for the preparation of $Cu(OH)_2$ nanowires. The reaction for the production of $Cu(OH)_2$ can be described as follows:

$$Cu+4NaOH+(NH_4)_2S_2O_8 \rightarrow Cu(OH)_2 + Na_2SO_4 + 2NH_3\uparrow +2H_2O$$

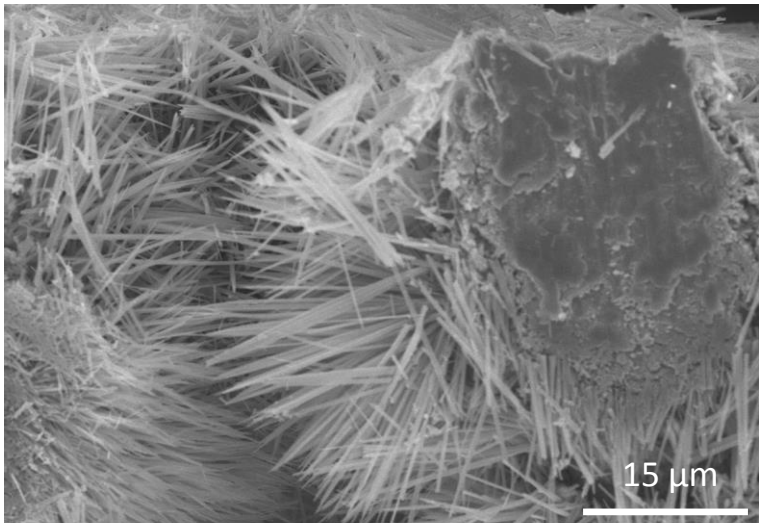

Figure S2. Cross-section view of the copper lines after growth of nanostructures, it can be seen that the average length of the $Cu(OH)_2$ nanowires is about 20 µm.

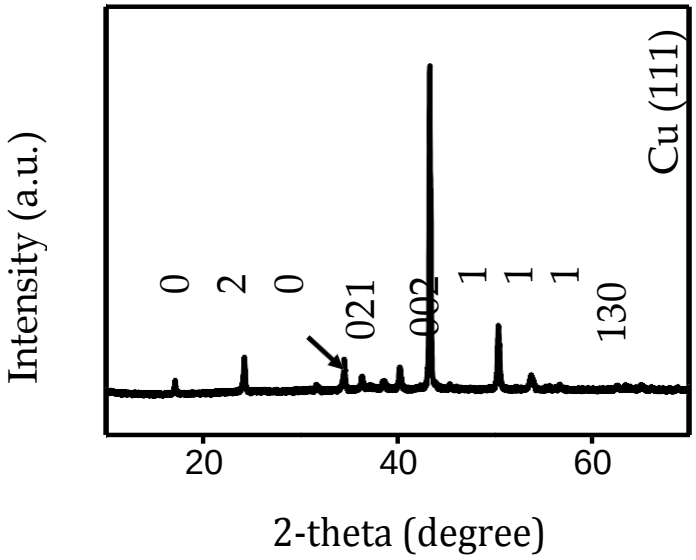

Figure S3. XRD patterns of the film, it can be seen that all peaks (except those ascribed to the Cu substrate) can be ascribed to the $Cu(OH)_2$. X-ray diffraction data was collected using an X-ray diffractometer (D8 Advance, Bruker) with Cu Ka radiation (λ=1.5418 Å).

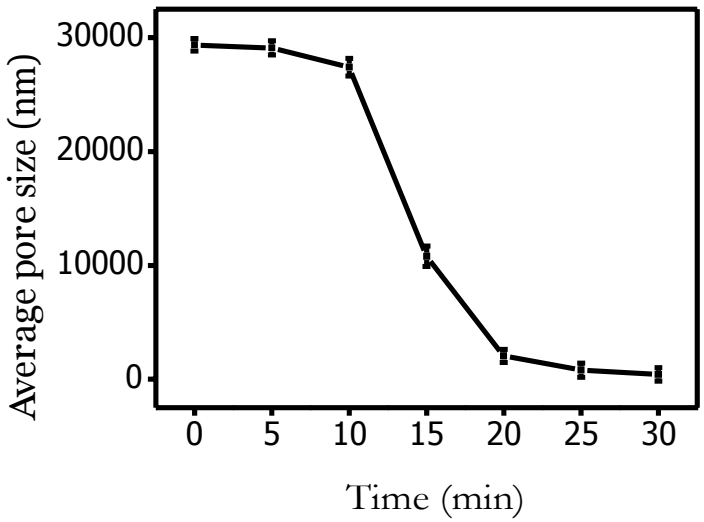

Figure S4. Dependence of pore size on the reaction time for production of $Cu(OH)_2$ nanowires. It can be seen that as the time is increased, the average pore size is decreased. The pore size on the film was examined by a mercury porosimetry (Autopore 9500, Micromeritics).

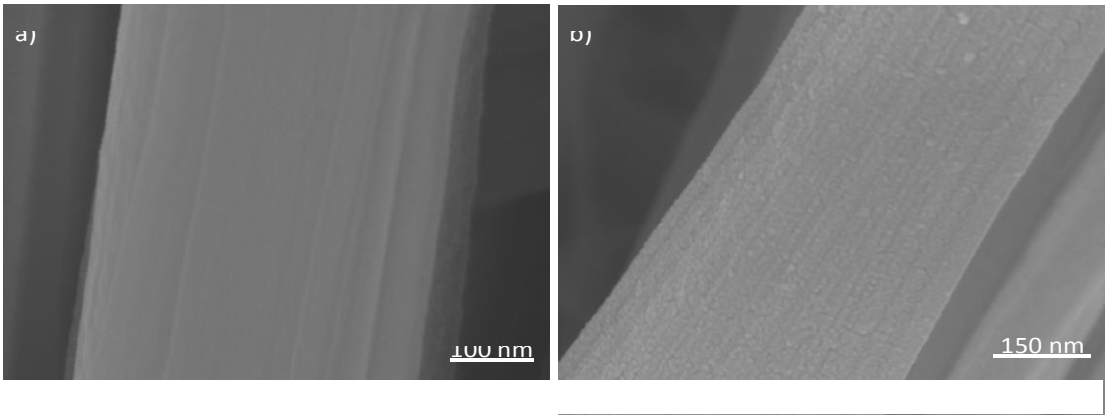

Figure S5. (a) and (b) SEM images of $Cu(OH)_2$ nanowire before and after coated with Au, respectively. Compared with picture (a), it can be seen that a layer of Au nanoparticles have been sputtered onto the $Cu(OH)_2$ nanowire.

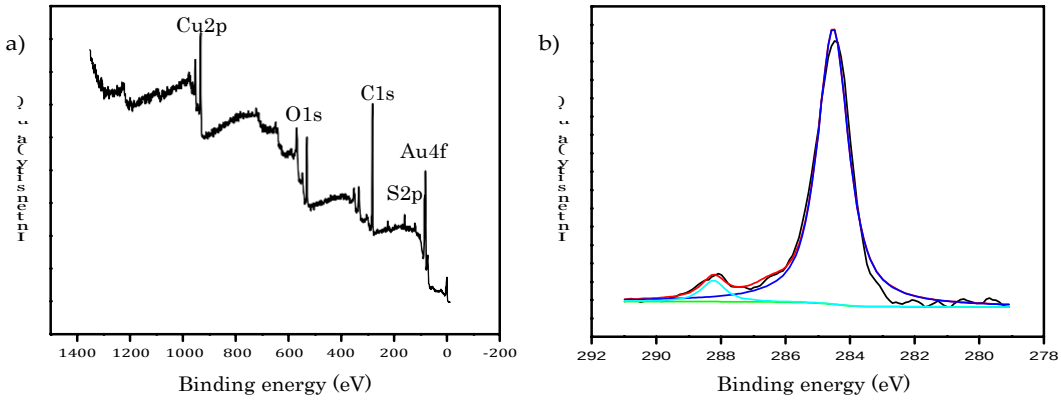

Figure S6. Ca3XPS survey of the surface, (b) high-resolution C1s XPS spectra of the surface (prepared with X_{COOH} = 0.6). The peak at 284.8 eV is ascribed to C-C/C-H, the peak at about 288.2 eV is ascribed to –COOH.

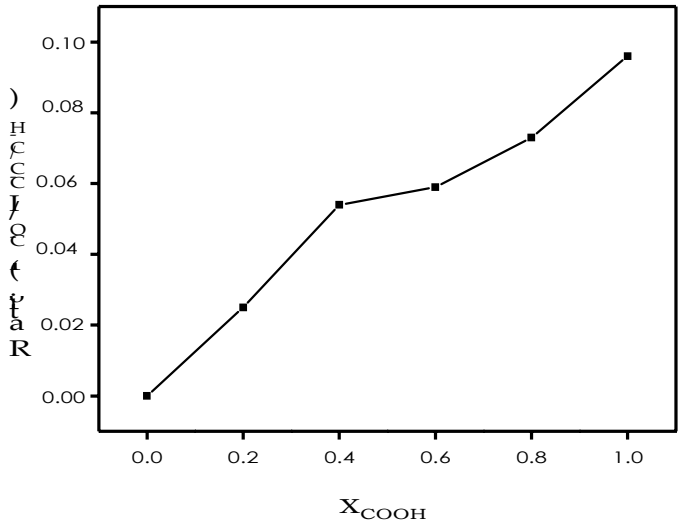

Figure S7. The relationship between the ratio of the C1s intensity of the carboxylic acid groups to that of alkyl carbons and the X_{COOH} in the modified solutions.

From Figure S7, it can be seen that the C1s peak intensity of carboxylic acid groups comparing with that of the alkyl carbons is increased as the X_{COOH} is increased (X_{COOH} is the mole fraction of $HS(CH_2)_{10}COOH$ in the modified solution), indicating that the modification method used in the paper is effective and the surface

composition can be controlled by changing the composition of the modified solution.

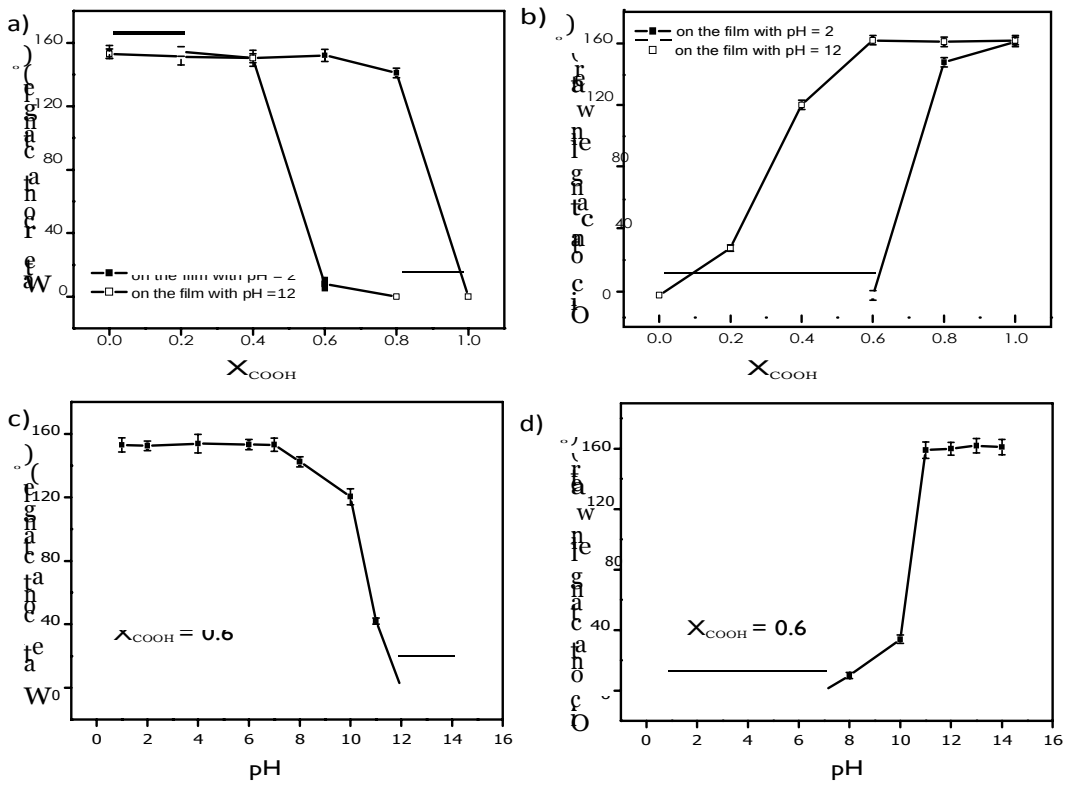

Figure S8. Dependence of water contact angles (a) and underwater oil (1, 2-dichloroethane) contact angles (b) on the X_{COOH} (mole fraction of $HS(CH_2)_{10}COOH$ in the modified solution). Dependence of water contact angle (c) and underwater oil contact angle (d) on water pH for film prepared with X_{COOH} = 0.6.

It can be seen that the transition from the superhydrophobicity/superoleophilicity to the superhydrophilicity/underwater superoleophobicity can be realized on the film prepared with X_{COOH} = 0.6. In addition to the reversibility, we also investigated the relationship between the contact angles and the water pH. It can be seen that for acidic water and neutral water, the film shows superhydrophobicity. When the water pH is further increased, the contact angles would be decreased, and when the pH is about 12, the film shows superhydrophilicity. In addition to water, oil contacts in water were

also investigated as a function of water pH. One can observe that in non-basic water, film shows underwater superoleophilicity, as the water pH is increased, the oil contact angled would be increased, and the water pH is higher than 11, the film would show superoleophobicity.

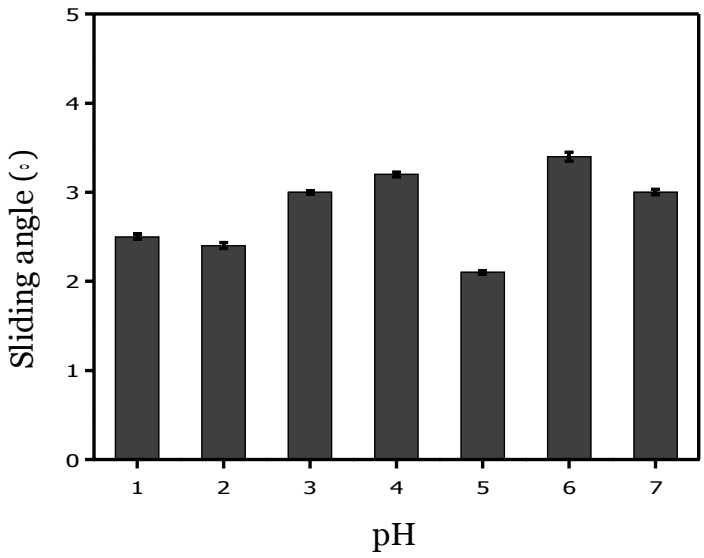

Figure S9. Statistic of sliding angles of water with different pH on the film.

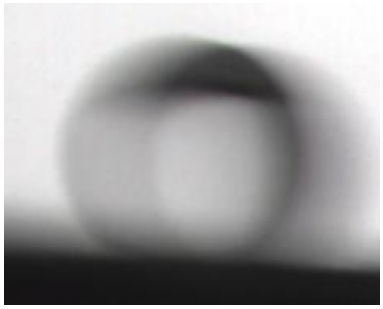

Figure S10. An oil droplet (1, 2-dichloroethane) rolling away the film in basic water (pH = 12) with a sliding angle of about 2°.

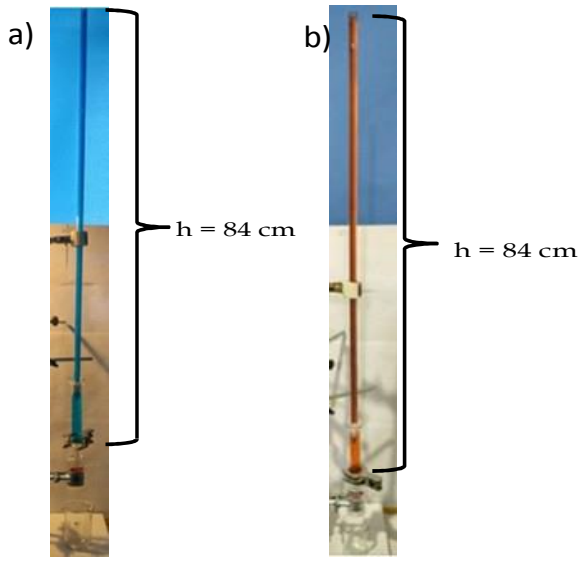

Figure S11. Testing device for intrusion pressure: a) water on the superhydrophobic/superoleophilic film; b) oil (hexane) on the basic water prewetted superhydrophilic/underwater superoleophobic film. In this work, by using the above device, different liquid intrusion pressures were investigated. As shown in Figure S11a, for the as-prepared superhydrophobic/superoleophilic film, water cannot pass through the film even when the glass tube (84 cm length) was full of water, indicating that the intrusion pressure for water on the film is higher than 8.4 KPa (calculated by equation 1 in paper). As the oil is used, it can permeate the film spontaneously, demonstrating a low oil intrusion pressure. When the film is prewetted with basic water (pH = 12), the water intrusion pressure is decreased, and water can pass through the film under the gravity. The decrease of water intrusion pressure is ascribed to the transition of film wettability to the superhydrophilic state. Whereas for oil, different from the original film, after prewetted by basic water, oil intrusion pressure is increased apparently. As shown in Figure S11b, oil (hexane) has the similar phenomenon with the water on the original film, indicating that the film has a high oil

intrusion pressure (higher than 5.8 KPa). Other oils including toluene, gasoline, petroleum ether, chloroform were also used to investigated, and the results please see Table S2

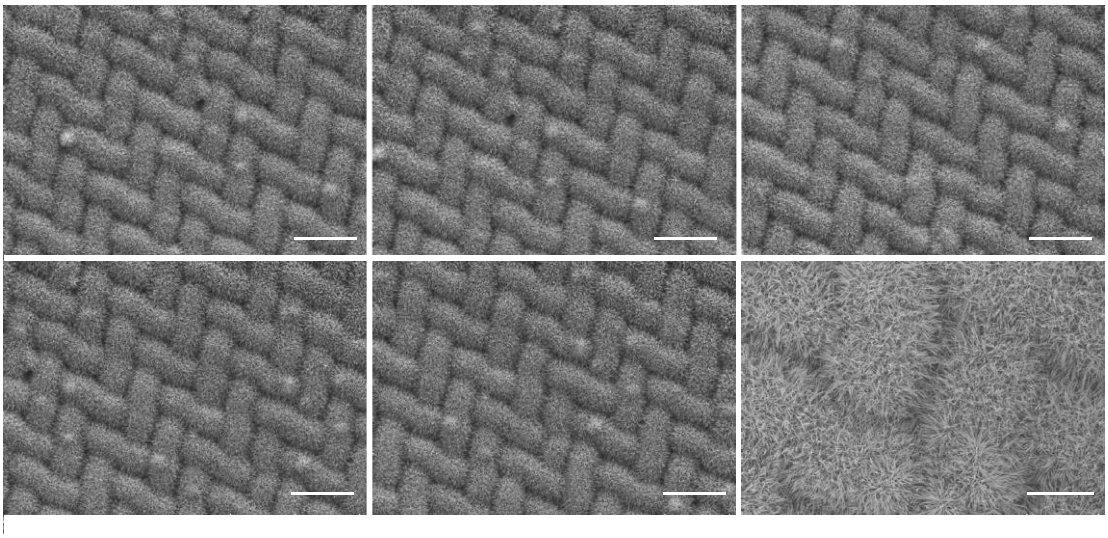

Figure S12. SEM images of superhydrophobic/superoleophilic film after immersion into different oils for about 24 h: (a) hexane; (b) chloroform; (c) gasoline; (d) toluene; (e) petroleum ether, respectively. (f) is the magnified image of (e), which is similar with the magnified images of (a-d). From these pictures, one can observe that after immersion into these oils, the surface microstructures have no apparent variation compared with the original film (Figure 1)

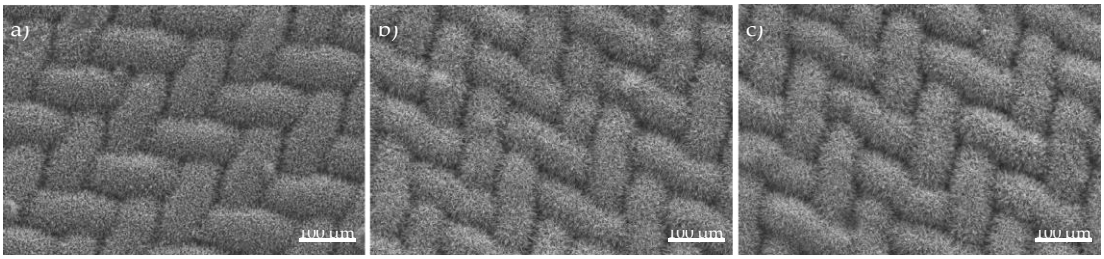

Figure S13. SEM images of superoleophilic/underwater superoleophobic film after immersion into different water solutions for about 24 h: (a) pH = 4, (b) pH = 14, (c) 10%wt NaCl. It can be seen that after immersion into these solutions, the

nanostructures have no apparently variation, means that the film has a good anti-corrosive ability.

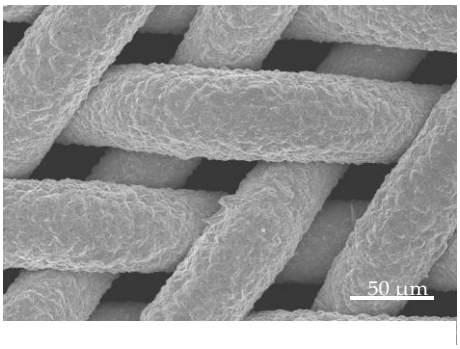

Figure S14. SEM image of the film after immersion into water with pH = 1 for about 24 h, it can be seen that the nanostructures disappeared after reaction. For water solutions with pH 2, and pH 3 have the similar phenomena.

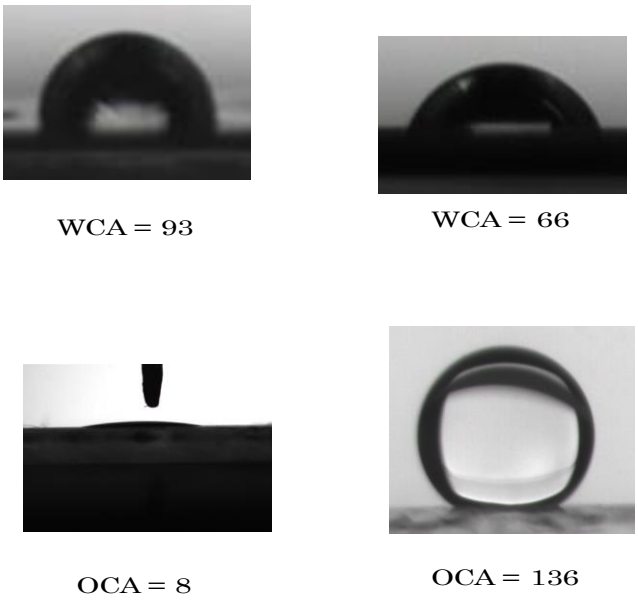

Figure S15. Shapes of a water droplet on the flat film prepared with X_{COOH} = 0.6: (a) pH =2; (b) pH = 12. (c) A 1, 2-dichloroehtane droplet on the same flat film in air (c) and in water with pH = 12 (d), respectively.

Table S1. Sizes of emulsified droplets for different emulsions.

	Surfactant-free droplet sizes (μm)		Surfactant-stabilized droplet sizes (μm)	
	Water-in-oil	Oil-in-water	Water-in-oil	Oil-in-water
Toluene				
Hexane				
Chloroform				
Petroleum ether				
Gasoline				

Table S2. Results of intrusions for different oils on the basic water (pH = 12) prewetted superhydrophilic/underwater superoleophobic film.

	Intrusion pressure (KPa)
Toluene	
Hexane	
Chloroform	
Petroleum ether	
Gasoline	